Indian Journal of Pure & Applied Physics
Vol. 59, February 2021, pp. 92-102

Study on crystalline phases and degree of crystallinity of the melt compounded PVA/MMT and PVA/PVP/MMT nanocomposites

Shobhna Choudhary[*a], Priyanka Dhatarwal[b] & R J Sengwa[b]

[a]CSIR- Human Resource Development Centre, Ghaziabad – 201 002, India

[b]Dielectric Research Laboratory, Department of Physics, Jai Narain Vyas University, Jodhpur 342 005, India

Received 7 October 2020; accepted 4 December 2020

Polymer nanocomposite (PNC) films comprised poly(vinyl alcohol) (PVA) and also its blend with poly(vinyl pyrrolidone) (PVP) (*i.e.,* PVA/PVP = 75/25 wt/wt%) as host matrices loaded with different amounts of montmorillonite (MMT) nanoclay up to 10 wt% were prepared by melt compounded method. X-ray diffraction (XRD) patterns of these PNC films were recorded in the appropriate angular range of 2θ values 3.8°–26° for their crystalline phase structural characterization. In comparison to the broader-type single diffraction peak for the aqueous solution cast prepared pure PVA film and that of the PVA/PVP blend film which is attributed to the hydrogen bonded isotactic and syndiotactic PVA crystals, five sharp diffraction peaks of different intensities corresponding to the evolution of various crystallites in the melt compounded PVA and PVA/PVP blend films were observed. Further, these peaks intensities were found significantly affected by the amounts of loaded MMT in these polymer matrices-based nanocomposites. It was observed that the prominent crystalline phase of the pure PVA converted into alternative tactic phases in the PVA/MMT films with the variation of MMT concentration. The prime crystalline phase of the PVA/PVP/MMT nanocomposites underwent alternative crystal structures formation abruptly on the initial loading of the 1 wt% amount of MMT in the PVA/PVP blend matrix reflecting a substantial alteration in the direction and nature of hydrogen bonding within the PVA crystal structures, and less changes were found with the further increase of MMT concentration up to 10 wt%. The effect of MMT loading on the crystallite sizes, degree of crystallinity, and the exfoliated and intercalated MMT structures in these PNC materials were analyzed in detail.

Keywords: Poly(vinyl alcohol), Poly(vinyl pyrrolidone), Nanoclay, Nanocomposites, Crystallinity, X-ray diffraction

1 Introduction

Preparation and characterization of the polymer matrix and clay nanofiller based polymer nanocomposites (PNCs) have been established as one of the important field of researches in the advances of polymer materials science and technology[1–9]. Results of various studies on the PNCs confirmed that the loading of nanoclay into a polymer matrix formed highly improved properties flexible materials, which are used in the development of daily-use products as well as the advanced flexible-type various devices[3–6, 9, 10]. The improvement in properties of such materials is mainly being governed by the formation of intercalated/exfoliated nanoplatelets of the clay as affected by their ion-dipole and dipole-dipole interactions with the different functional groups of the polymers chains[3, 4, 9, 10]. In the last two decades, PNCs based on several synthetic and natural polymers matrices with a variety of clays loading had been prepared and examined in search of their promising mechanical, thermal, dielectric, electrical, inflammable, anticorrosion, permeable, structural, and many other useful technological properties[2–15].

Among the hydrophilic and biodegradable-type synthetic polymers, the poly(vinyl alcohol) (PVA) and the poly(vinyl pyrrolidone) (PVP) have proved enormous technological and pharmaceutical applications because of their excellent solubility in water, low toxicity, and good compatibility with different fillers/dopants[16–25]. The solution cast prepared films of these polymers have high optical transparency, which promotes their use as binder and host matrix in the preparation of a variety of advanced optoelectronic materials[20–26]. The PVA is semicrystalline in nature, and crystallinity of its film immensely depends on the film preparation method and any subsequent annealing treatment[27–30]. In contrast to the PVA film, the PVP film is an amorphous and slightly brittle on blending and also has organic glassy look[23–25]. The functional groups of these polymers *i.e.*, the hydroxyl groups in the repeat units of PVA chain and

Corresponding author
(E-mail: shobhnachoudhary@rediffmail.com)

the carbonyl group in the monomer units of PVP chain exhibit strong tendency of interactions with the most of organic/inorganic nanofillers and a variety of dopants which ultimately result in formation of promising complexes and the composites for their uses in advanced technologies[20–25, 31–33].

Due to appreciable ability of the ion-dipole and dipole-dipole type interactions of the PVA and the PVP with the surface charges of the platelets of montmorillonite (MMT) nanoclay, the MMT nanoplatelets loaded colloids, hydrogels, and the solid flexible films of these polymers remains an intense area for several investigators[16, 17, 29, 30, 34–40]. Over the last two decades, extensive research has been conducted on the PVA/PVP blends for confirmation of their promising tailorable properties as biodegradable polymer blend matrix appropriateness in order to make them more appealing in designing of advanced functional materials with polymer technology[41–47]. It has already been investigated that the structural properties of the solution cast PVA/PVP blend films of various compositions are mainly governed by the formation of dipolar interactions between various polymers functional groups[43, 45–47].

Besides the use of solution casting method in the polymer film preparations, the PVA film can also be easily prepared by the direct melt compounding method. Because both these methods are equally suitable in the film preparation by the technological industries, the PVA is commonly used as binder in the fabrication of composite materials as per requirement either by the melt compounding or by the solution cast method for the different applications[16, 17, 20–22]. For the melt compounded composites of the PVA with MMT, the studies on the growth of the crystals in the PVA matrix and the filler contents effect on the degree of crystallinity of the nanocomposites materials have not been conducted to the best of our knowledge.

Keeping this fact in mind, we have made an attempt to characterize the nature of crystals formed in the melt compounded films of the PVA, PVA/PVP blend, and their nanocomposites with the MMT nanofiller in relation to confirmation of their structural properties and the degree of crystallinity by assuming these as model academic composite materials. The –OH groups of PVA in its molten state can interact directly with the C=O groups of PVP which have resulted in their good miscibility, and also interactions of these groups with the Na^+ ions and siloxane group of the MMT caused successful nanocomposite formation. Therefore these melt compounded materials exhibited some unique structural properties explored in detail in the present study as compared to their solution cast composite films investigated earlier[14, 17, 43].

2 Experimental Section

2.1 Materials

The PVA (M_w = 77000 $gmol^{-1}$) and PVP (M_w = 24000 g mol^{-1}) powders of analytical grade were purchased from Loba Chemie, and S.D. Fine-Chem, both of India, respectively. The polymer grade hydrophilic montmorillonite (MMT) clay (Nanoclay, PGV), a product of Nanocor®, was purchased from Sigma-Aldrich, USA. As per technical specifications of the manufacturer, the MMT was white in colour, and had 145 meq/100g cation exchange capacity (CEC), 150–200 aspect ratio (length/breadth), 2.6 g/cc specific gravity, and 9–10 pH value in a 5% dispersion and also it is recommended as the best clay for the preparation of nanocomposites with the PVA matrix.

2.2 Sample Preparation

The compositional ratio of PVA/PVP blend used was 75/25 (wt/wt %). The films of pristine PVA, PVA/PVP blend, and their nanocomposites with MMT nanofiller were prepared by melt compounding process using a hot compression polymer press (TechnoSearch Instruments; Model PF M 15). In this process, firstly, the PVA or the agate mortar and pestle mixed PVA/PVP composition were melted in the 60 mm diameter circular stainless steel die with fixed spacer at 230 °C. The melt polymer material was pressed under 3 tons pressure and subsequently cooled to room temperature using the controlled cooling arrangement in the die which resulted the rigid-type polymer film. For the preparation of PVA/*x* wt% MMT and PVA/PVP/*x* wt% MMT nanocomposites having *x* values = 1, 2, 3, 5, and 10, initially the required amounts of MMT nanopowder for various concentrations were mixed into the respective amounts of polymer powder using an agate mortar and pestle. After that each composition was blended by high energy planetary ball mill in the agate vessel with agate balls at the 200 rpm for 10 min duration to achieve the homogenous mixture. Finally, the direct melt compounding of each mixture was performed in the polymer press. The aqueous

solution cast films of PVA, PVP, and PVA/PVP blend were prepared by dissolving these polymers in deionised water and then casting into the petri dishes. These solution cast films were vacuum dried prior to their measurements.

2.3 Characterization

The XRD patterns of the MMT nanopowder, the pristine polymer, and polymer blend films, and the PNC films were recorded in reflection mode using a PANalytical X′pert Pro MPD. The CuK_α X-ray radiation of wavelength $\lambda = 1.5406$ Å was generated by applying tube voltage of 45 kV and current of 40 mA. Scan step was kept 0.05 deg/s for recording the XRD traces. The powder of MMT was tightly filled in the sample holder, while each film was fixed on top of the sample holder during their XRD recording in the useful angular range of 2θ from 3.8° to 26°. The XRD patterns of the PVA/*x* wt% MMT and PVA/PVP/*x* wt% MMT nanocomposites recorded at room temperature are shown in Figs. 1 and 2, respectively. These traces are set vertically for their clarity and better comparison. The scans were repeated on some of the representative samples which were prepared separately by following the same processing steps, and their excellent reproducibility was noted.

The values of the various diffraction peaks positions 2θ, their intensity *I* (counts), and full width at half maximum FWHM or β (the broadening of peak at half-height expressed in radians of 2θ, *i.e.* width measured in 2θ degrees and then multiplied by π/180) of the measured materials were determined

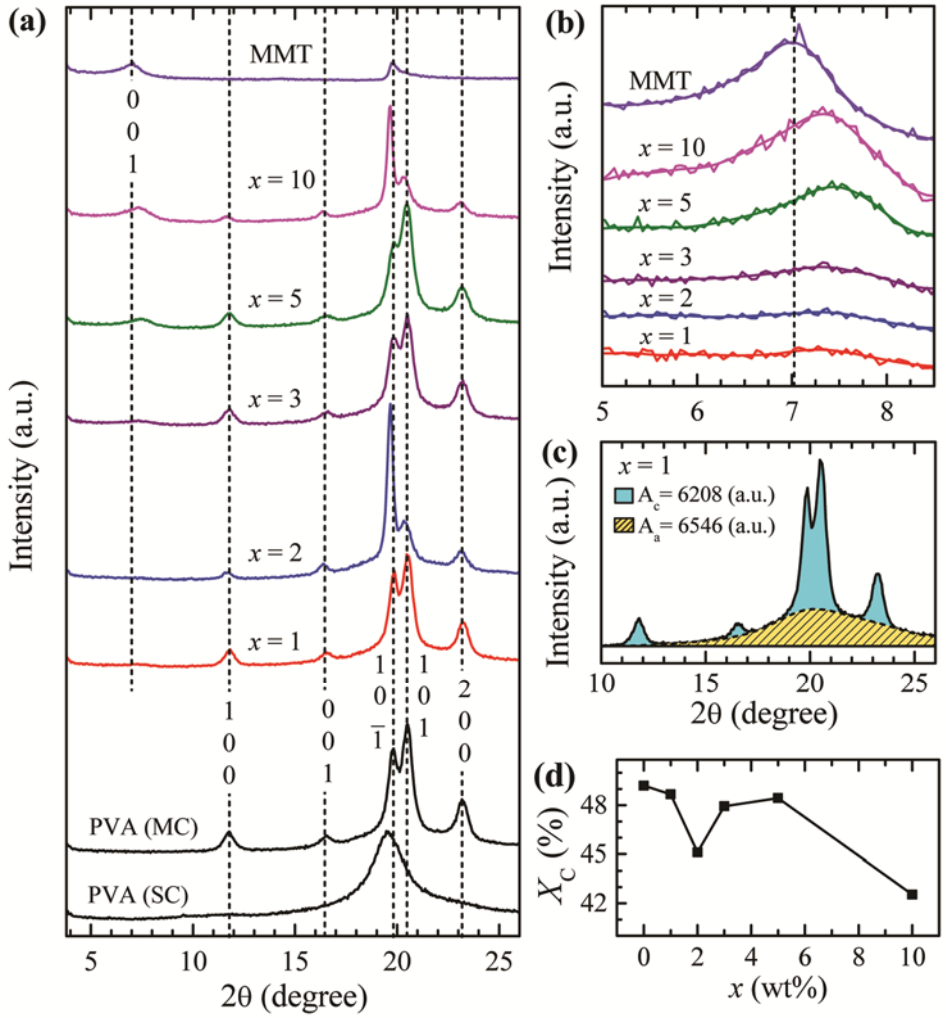

Fig. 1 — (a) XRD patterns of MMT powder, PVA (SC), PVA (MC), and PVA/*x* wt% MMT nanocomposite (*x* = 1, 2, 3, 5 and 10) films, (b) Zoom scale with smoothing by FFT filter of the 001 peak of pure MMT and various *x* (wt%) nanocomposites, (c) XRD trace for 1 wt% of MMT concentration PNC film as representative for procedure of the determination of A_c and A_a values for the crystallinity X_c, and (d) the plot of X_c (%) versus the *x* (wt%) concentration of the PNC films.

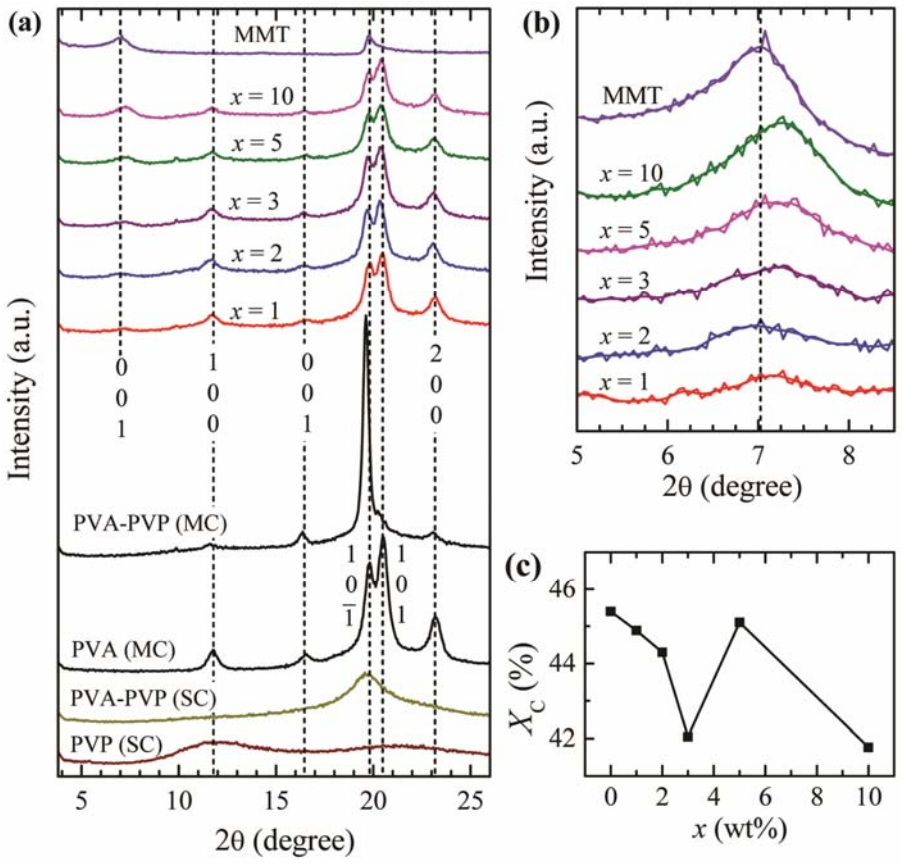

Fig. 2 — (a) XRD patterns of MMT powder, PVP (SC), and PVA/PVP blend film (SC), PVA (MC), and the PVA/PVP/*x* wt% MMT nanocomposite (*x* = 1, 2, 3, 5 and 10) films, (b) Zoom scale with smoothing by FFT filter of the 001 peak of pure MMT and various *x* (wt%) nanocomposites, and (c) the plot of crystallinity X_c (%) versus the *x* (wt%) concentration of the PNC films.

from their XRD traces by using the X'pert pro® software. The structural parameters namely interlayer spacing *d*, crystallite size *L*, interchain separation *R*, and the degree of crystallinity X_c of these materials were computed using the following relations. The *d*-spacings of the various reflection planes of the crystals were determined by Bragg's relation Eq. 1:

$$d = \lambda / 2\sin\theta \quad \ldots (1)$$

The values of mean crystallite size *L* in the direction perpendicular to *hkl* planes of various crystal phases in these nanocomposites were determined by Scherrer's relation Eq. 2:

$$L = 0.94\lambda / \beta\cos\theta \quad \ldots (2)$$

The values of interchain separation *R* was estimated by Eq. 3:

$$R = 5\lambda / 8\sin\theta \quad \ldots (3)$$

The degree of crystallinity X_c of the PVA structures in these PNCs were computed using the crystalline peaks area (A_c) and the hump area (A_a) in the relation Eq. 4:

$$X_c\,(\%) = (A_c / (A_c + A_a)) \times 100 \quad \ldots (4)$$

The observed values of 2θ, *d*, FWHM, *L*, *I*, and *R* corresponding to each reflection plane peak noted in the PVA/*x* wt% MMT and PVA/PVP/*x* wt% MMT nanocomposites are listed in Tables 1 and 2, respectively. The X_c (%) values of these nanocomposite materials are listed in Table 3.

3 Results and Discussion

3.1 PVA/x wt% MMT nanocomposites

Figure 1a shows the XRD patterns of the MMT nanopowder, aqueous solution cast (SC) prepared PVA film (*i.e.*, PVA (SC)), and the melt compounded (MC) prepared PVA film *i.e.*, PVA (MC) and that of the PVA/*x* wt% MMT nanocomposite films.

Table 1 — Bragg's angle 2θ, basal spacing *d*, full width at half maximum FWHM, crystallite size *L*, intensity *I*, and interchain spacing *R* corresponding to 001 peak of MMT and various crystalline reflection plane peaks of the PVA crystals in the melt compounded PVA/*x* wt% MMT nanocomposite films.

x (wt%)	2θ (deg)	*d* (nm)	FWHM (rad)	*L* (nm)	*I* (counts)	*R* (nm)
001 reflection peak of MMT						
MMT	7.028	1.257	0.0172	8.44	520	1.571
1	7.28	1.213	0.0137	10.56	68	1.517
2	7.16	1.234	0.0082	17.61	80	1.542
3	7.33	1.205	0.0100	14.51	136	1.506
5	7.44	1.187	0.0137	10.56	307	1.484
10	7.34	1.203	0.0137	10.56	458	1.504
100 reflection peak of PVA						
PVA	11.76	0.751	0.0051	28.27	870	0.940
1	11.79	0.750	0.0077	18.82	726	0.938
2	11.68	0.757	0.0068	21.16	285	0.946
3	11.80	0.749	0.0034	42.34	687	0.937
5	11.78	0.750	0.0094	15.41	579	0.938
10	11.65	0.758	0.0068	21.16	224	0.949
001 reflection peak of PVA						
PVA	16.55	0.535	0.0068	21.28	366	0.669
1	16.56	0.534	0.0068	21.28	295	0.669
2	16.39	0.540	0.0068	21.27	390	0.676
3	16.57	0.534	0.0102	14.21	257	0.668
5	16.54	0.535	0.0102	14.21	259	0.669
10	16.38	0.540	0.0060	24.36	250	0.676
$10\bar{1}$ reflection peak of PVA						
PVA	19.80	0.448	0.0051	28.55	4146	0.560
1	19.85	0.446	0.0051	28.55	3755	0.559
2	19.67	0.450	0.0042	34.23	7585	0.564
3	19.84	0.447	0.0068	21.37	3466	0.559
5	19.87	0.446	0.0051	28.55	3375	0.558
10	19.66	0.451	0.0042	34.23	5056	0.564
101 reflection peak of PVA						
PVA	20.51	0.432	0.0068	21.40	5358	0.541
1	20.53	0.432	0.0068	21.40	4525	0.540
2	20.37	0.435	0.0042	34.26	2102	0.545
3	20.50	0.432	0.0068	21.40	4550	0.541
5	20.48	0.433	0.0085	17.13	5132	0.542
10	20.33	0.436	0.0051	28.57	1709	0.546
200 reflection peak of PVA						
PVA	23.19	0.383	0.0077	19.12	1937	0.479
1	23.23	0.382	0.0094	15.65	1536	0.478
2	23.12	0.384	0.0060	24.61	827	0.480
3	23.18	0.383	0.0094	15.65	1524	0.479
5	23.18	0.383	0.0085	17.21	1336	0.479
10	23.14	0.384	0.0068	21.49	609	0.480

Table 2 — Bragg's angle 2θ, basal spacing *d*, full width at half maximum FWHM, crystallite size *L*, intensity *I*, and interchain spacing *R* corresponding to 001 peak of MMT and various crystalline reflection plane peaks of the PVA crystals in the melt compounded PVA/PVP/*x* wt% MMT nanocomposite films.

x (wt%)	2θ (deg)	*d* (nm)	FWHM (rad)	*L* (nm)	*I* (counts)	*R* (nm)
001 reflection peak of MMT						
MMT	7.028	1.257	0.0172	8.44	520	0.571
1	7.13	1.238	0.0102	14.09	96	0.549
2	7.01	1.259	0.0137	10.56	125	0.575
3	7.14	1.237	0.0171	8.44	155	0.546
5	7.22	1.223	0.0137	10.56	218	0.529
10	7.26	1.216	0.0068	21.10	442	0.521
100 reflection peak of PVA						
PVA	11.76	0.751	0.0051	28.27	870	0.940
PVA–PVP	11.62	0.760	0.0068	21.16	206	0.951
1	11.70	0.755	0.0051	28.27	488	0.945
2	11.65	0.758	0.0102	14.13	465	0.949
3	11.70	0.755	0.0085	16.95	470	0.945
5	11.71	0.755	0.0068	21.16	371	0.944
10	11.72	0.754	0.0085	16.95	295	0.943
001 reflection peak of PVA						
PVA	16.55	0.535	0.0068	21.28	366	0.669
PVA–PVP	16.34	0.542	0.0042	34.07	444	0.678
1	16.58	0.534	0.0085	17.04	126	0.668
2	16.46	0.538	0.0102	14.20	113	0.673
3	16.44	0.538	0.0068	21.27	191	0.673
5	16.52	0.536	0.0102	14.21	117	0.670
10	16.45	0.538	0.0051	28.41	119	0.673
$10\bar{1}$ reflection peak of PVA						
PVA	19.80	0.448	0.0051	28.55	4146	0.560
PVA–PVP	19.63	0.451	0.0051	28.54	9683	0.565
1	19.82	0.447	0.0060	24.48	2443	0.559
2	19.69	0.450	0.0051	28.54	2448	0.563
3	19.73	0.449	0.0042	34.23	2483	0.562
5	19.78	0.448	0.0060	24.48	1878	0.561
10	19.77	0.448	0.0060	24.48	1724	0.561
101 reflection peak of PVA						
PVA	20.51	0.432	0.0068	21.40	5358	0.541
1	20.47	0.433	0.0060	24.51	2809	0.542
2	20.35	0.436	0.0068	21.39	2873	0.545
3	20.40	0.434	0.0068	21.39	2956	0.544
5	20.42	0.434	0.0094	15.58	2157	0.543
10	20.42	0.434	0.0060	24.50	2260	0.543
200 reflection peak of PVA						
PVA	23.19	0.383	0.0077	19.12	1937	0.479
PVA–PVP	23.06	0.385	0.0068	21.49	349	0.482
1	23.19	0.383	0.0077	19.12	1004	0.479
2	23.07	0.385	0.0068	21.49	1038	0.482
3	23.10	0.384	0.0034	42.98	1052	0.481
5	23.13	0.384	0.0068	21.49	814	0.480
10	23.15	0.383	0.0068	21.49	754	0.480

Table 3 — Values of degree of crystallinity X_c (%) of the solution cast PVA (SC) and PVA/PVP (SC) films, and the melt compounded PVA (MC), PVA/PVP (MC), and the PVA/*x* wt% MMT and PVA/PVP/*x* wt% MMT nanocomposite films.

Films	X_c (%)	Films	X_c (%)
PVA (SC)	41.7	PVA/PVP (SC)	30.5
PVA (MC)	49.2	PVA/PVP (MC)	45.4
PVA/*x* wt% MMT		PVA/PVP/*x* wt% MMT	
x (wt%)	X_c (%)	*x* (wt%)	X_c (%)
1	48.7	1	44.9
2	45.1	2	44.3
3	47.9	3	42.1
5	48.4	5	45.1
10	42.5	10	41.8

The facts on the structural characteristics from the XRD pattern are the peaks show the presence of crystals in the material, the peak positions are related to the crystal phases present, the peak height indicate the phase concentration, the peak width is associated with the crystallite size, and the background hump confirms the amount of amorphous content in the semicrystalline material. The characteristics features of the XRD patterns of these materials, given in Fig. 1a, are (i) the MMT nanopowder exhibited two peaks at 2θ values 7.03° and 19.79° which correspond to its 001 and 101 crystal reflection planes and these are noted in good agreement with the earlier studies[14, 29, 34], (ii) the aqueous solution cast PVA (SC) film showed only one broader-type peak centered at 19.56° which can be assigned to its concurrent crystal reflections $10\bar{1}$ and 101[27, 34], (iii) the melt compounded PVA (MC) film exhibited five peaks of different intensities which are centered at 2θ values of 11.76°, 16.55°, 19.80°, 20.51°, and 23.19° corresponding to the reflection planes indices 100, 001, $10\bar{1}$, 101, and 200 representing the sydiotactic and isotactic crystallites of the PVA unit cell consisted of two atactic chains with 50% occupancy of the –OH sites as described in the literature[27]. These peaks have good resemblance, both in their positions and relative intensities with the XRD trace of PVA film prepared by aqueous solution cast method and then annealed at 230 °C[27, 28]. And (iv) the changes in the intensities of the PVA peaks with the change of MMT concentration in the PVA/*x* wt% MMT nanocomposites confirmed the interactions existed between the silanol groups (Si–O) of the MMT nanoplatelets and the hydroxyl groups (–OH) of the PVA repeat units in these melt compounded prepared nanocomposites as also demonstrated in the literature[27, 29].

It can be noted from Fig. 1a that the aqueous solution cast PVA (SC) film has only one broad peak of intensity counts 3601, which has resolved into relatively sharper doublet peaks corresponds to $10\bar{1}$ and 101 reflection planes with their relative intensities 4146 and 5358, respectively (see Table 1), when it was processed by compression molding from the molten state. Further, in addition to these characteristic doublets, the appearance of additional peaks of relatively low intensities corresponding to 100, 001, and 200 crystal planes confirmed the increase in degree of crystallinity of the melt processed PVA film as compared to its solution cast film. Earlier, it was reported that the solution cast PVA film has around 30% crystalline phase, whereas the degree of crystallinity (X_c) was increased and noted in the range 38–50% for the solution cast PVA films when these were annealed and cooled to room temperature with increasing temperature in steps from 120 to 230 °C[27]. In this study, we found the X_c values of 41.7% and 49.2% for the PVA films prepared by SC and MC methods, respectively. This finding on the melt compounded PVA film is in agreement with the crystallinity behaviour of the annealed PVA film up to 230 °C which was initially prepared by solution casting[27]. It may be because of the fact that the annealing temperature is the same as we kept in the preparation of direct melt compounded PVA film from the powder. Furthermore, the concerted $10\bar{1}$ and 101 crystal peaks is the basis of centered single peak of decreased intensity appeared in the solution cast PVA film.

The comparative analysis of the diffraction traces of PVA/*x* wt% MMT nanocomposites (Fig. 1a) revealed that there were noticeable changes in the peaks intensities corresponding to the various reflection planes of the PVA crystals when the concentration of MMT nanofiller was increased gradually up to 10 wt% in the PVA host matrix. Here, first we consider the 001 reflection plane peak intensity of the MMT in the PNC films as shown separately in Fig. 1b with the zoom scale and smoothing made by using the Fast Fourier Transform (FFT) filter facility available in the Origin software. This peak intensity is found gradually enhancing (see Table 1) confirming the homogeneous distribution of MMT in the PVA matrix and there is the successful

formation of these nanocomposites as explained for several other kinds of PNCs from their XRD results[23–25]. In general, the exfoliated MMT structures does not exhibit the 001 peak and for the intercalated structures in the PNCs this peak appear at the lower angle in comparison to the pristine MMT[14, 15, 29]. But for these melt compounded PVA/*x* wt% MMT films, this peak position is found very close to that of the pristine MMT which indicates that some aggregated MMT tactoids exist in these PNC films which may be due to the processing of melted material to form a film under pressing. Further, the intensity of 001 peak of MMT for its 10 wt% loading in the PVA matrix was found almost same as of the pristine MMT nanopowder which inferred that some new crystal structures next to the MMT surfaces were formed because of the tendency of the PVA polar chains to completely cover the tactoids with an improvement in crystal perfection[29].

It can be understood from Table 1 that the variation in PVA peaks intensities corresponding to different reflection planes of the PVA/*x* wt% MMT nanocomposites changes unevenly with the increase of MMT concentration. At the 1 wt% loading of MMT nanoplatelets in the PVA matrix resulted similar-type of XRD pattern as of the PVA film with a slight decrease in the peaks intensities. However, at the 2 wt% of MMT loading, there was a huge increase in the intensity of $10\bar{1}$ peak with a significant decrease in 100 peak intensity. Simultaneously, a significant decrease in intensities of the 100 and 200 peaks were also noted which suggested a considerable variation in the direction and nature of hydrogen bonding within the crystal structure of the PVA as disclosed earlier[27]. Further increase of MMT concentration has produced the variations in intensities of 100 and 200 reflection peaks in the same manner, but $10\bar{1}$ and 101 peaks intensities has exhibited reverse trend (see Fig. 1a and Table 1), which evidences that as the crystal perfection in the $10\bar{1}$ reflection plane increases, simultaneously, there was a decrease in the 101 reflection plane. It is because of the fact that the increasing sharpness of a peak reflects the improved packing within the crystals and/or the phase concentration which was interpreted earlier in regards to improvement in the crystal perfection[27]. The effect of MMT loading on the 001 crystalline reflection plane of the PVA crystals was found relatively low in these PNC materials. These observations indicated that there were significant changes in the direction and nature of hydrogen bonding within the crystals which directly evidences some variations in the interactions between the PVA chains and the MMT nanoplatelets as the nanofiller concentration was gradually varied in the PVA/*x* wt% MMT nanocomposites.

The *d*-spacing values corresponding to 100, 001, $10\bar{1}$, 101, and 200 reflection planes of the crystals in the melt compounded PVA film were found 0.751, 0.535, 0.448, 0.432, and 0.383 nm, respectively (see Table 1). But significant variation was not observed in the *d*-spacing values of the PVA/*x* wt% MMT nanocomposites with the increase of MMT concentration up to 10 wt%. However, it was noticed that the crystallite sizes *L* of these nanocomposites changed anomalously with the variation of MMT concentration. Further, the *L* values corresponding to different reflection planes of the PVA crystals in the nanocomposites were found in the wide range of 14.21–42.34 nm.

The degree of crystallinity of the solution cast PVA (SC) film is found 41.7 % which is about 7 % lower than that of the melt compounded PVA (MC) film (49.2 %) (see Table 3). Fig. 1c demonstrates the procedure for the determination of A_c and A_a values from the XRD trace and then the crystallinity for the 1 wt% of MMT concentration PNC film as a representative sample. The variation of X_c for the PVA/*x* wt% MMT films with the MMT concentrations *x* (wt %) is shown in Fig. 1d. This figure explains that the crystallinity of the MMT loaded these PNC films is either close to that of the pristine PVA film or slightly lower than it *i.e.,* for 2 wt% and 10 wt% concentrations of the filler. This finding suggests that beside the significant alterations in the amount of crystalline phases, the crystallinity of the PVA/*x* wt% MMT films was less affected by the loading of MMT up to 10 wt%.

3.2 PVA/PVP/x wt% MMT nanocomposites

The XRD patterns of the melt compounded (MC) PVA film, PVA/PVP blend film, and PVA/PVP/*x* wt% MMT nanocomposite films along with aqueous solution cast (SC) PVP film and the PVA/PVP blend film and also the MMT nanopowder are depicted in Fig. 2a. Absence of sharp diffraction peaks in the XRD pattern of solution cast pure PVP film confirmed its amorphous nature[14]. Further, the PVP

exhibited two broad halos in the experimental range of 2θ which are centered at 12.04° and 22.56°, and these halos are found in agreement with its earlier reported XRD pattern[24, 25]. The aqueous solution cast PVA/PVP blend film had only one crystalline reflection peak of concurrent $10\bar{1}$ and 101 planes of the PVA crystallites with a significantly reduced intensity (1451 counts) as compared to the same reflection planes peak intensity of the aqueous solution cast pristine PVA film (3601 counts). This large decrease of PVA peak intensity confirms the formation of miscible PVA/PVP blend owing to hydrogen bond interactions exhibited between the functional groups of these polymers *i.e.,* the –OH groups of the PVA chain repeat units and the C=O groups of the PVP chain repeat units. As compared to the aqueous solution cast PVA/PVP blend film, the XRD trace of the melt compounded this polymer blend film had a sharp and highly intense peak at 2θ = 19.63° (see Fig. 2a) which reflects appreciable improvement in the PVA crystals perfection in the presence of PVP chains when the film was prepared through melt compounding.

In regards to the five reflection planes peaks (100, 001,$10\bar{1}$, 101, and 200) of melt compounded pure PVA film, the PVA/PVP blend film has four reflection peaks *i.e.* 100, 001, $10\bar{1}$, and 200 (see Fig. 2a). An enormous increase in the intensity of $10\bar{1}$ phase is the reason of 101 phase suppression in the PVA/PVP blend film. Further, a decrease in intensities of 100 and 200 peaks of the melt compounded PVA/PVP blend film as compared to the melt compounded pristine PVA film can be noted from Fig. 2a and Table 2. From these results it can be presumed that during the melt blending of high PVA amount with the less amount of PVP (*i.e.*, PVA/PVP =75/25 wt%), some favorable dipolar orientations occurred in the PVA molecular structures which strengthen the $10\bar{1}$ reflection plane packing within the PVA crystals and simultaneously this scratched the 101 crystalline reflection plane. The huge intensity of $10\bar{1}$ reflection plane also indicates the formation of supramolecular ordered miscible PVA/PVP blend domains by the adopted melt compounding preparation process of the blend film.

The shapes of XRD traces of PVA/PVP/*x* wt% MMT nanocomposites had good resemblance with that of the melt compounded pristine PVA film, and these PNCs traces differ significantly from the trace of melt compounded PVA/PVP blend film, which is interesting (see Fig. 2a). From these comparative traces, it can be noted that the presence of a little amount of MMT *i.e.*, 1 wt% in the blend matrix of PVA and PVP restricted the growth of supramolecular ordered PVA/PVP domains which was formed in the melt compounded film without nanofiller. It happened probably due to a large tendency of the PVP chain adsorption on the MMT surfaces through strong interactions between the C=O groups of the PVP and the surface hydroxyl groups of the MMT nanoplatelets, which made the PVP chains less interactive with the PVA chains in the presence of MMT nanosheets in the melt compounded prepared PVA/PVP/MMT nanocomposites. At the same time, the interactions between the PVA chains and the MMT nanoplatelets reduced the packing within the crystals which was reflected by the decrease in relative intensities of various reflection plane peaks (see Table 2). Furthermore, with the increase of MMT concentration from 1 to 3 wt%, additional small changes in the intensities of these peaks were found, but 5 and 10 wt% loading of MMT had resulted in a significant decrease of intensity values of all the crystalline reflection planes of the PVA/PVP blend. Fig. 2b showed the zoom of MMT 001 peak smoothened with the FFT filter which has gradual increase with the augment of MMT concentration in the PVA/PVP/*x* wt% MMT films. This finding confirms the successful formation of these nanocomposites as demonstrated for other inorganic nanofillers loaded PNC materials[22, 23, 25].

Table 2 shows that the *d*-spacing values of various crystal reflection planes of the PVA/PVP/*x* wt% MMT nanocomposites are almost independent of the MMT concentration, but their *L* values vary over a wide range of 14 nm to 43 nm, which confirm a huge alteration in the crystals domain sizes of the PVA structures in the PVA/PVP blend in the presence of MMT nanoplatelets. It can also be noted from the Tables 1 and 2 that *R* values for the PVA and PVA/PVP blend based PNCs have insignificant variation confirming that the packing of their structures has remained the same besides the initial loading of MMT and the increase of its concentration up to 10 wt%. Fig. 2c depicts the variation of X_c (%) with the MMT concentration *x* (wt%) for the PVA/PVP/*x* wt% MMT nanocomposites. The crystallinity of melt compounded PVA/PVP blend

film (X_c = 45.4%) is found about 4 % lower than that of the melt compounded pristine PVA film (X_c = 49.2%). But it is higher by about 15% as compared to the crystallinity of solution cast PVA/PVP blend film (X_c = 30.5%) which confirm that the melt compounding largely increased the crystallinity of the PVA-rich PVA/PVP blend. Further, the crystallinity of the solution cast PVA/PVP blend film (X_c = 30.5%) is found about 11% lower than that of the solution cast PVA film (X_c = 41.7%) which is expected due to the addition of amorphous PVP amount in the PVA-rich PVA/PVP blend. Further, Fig. 2c also demonstrates that there was a little and anomalous variation in the X_c values of the PVA/PVP/*x* wt% MMT films with the increase of MMT concentration. Furthermore, the X_c values of the melt compounded PVA/PVP/*x* wt% MMT films at all the concentrations of MMT were found slightly lower than that of the respective concentration melt compounded PVA/*x* wt% MMT films (see Table 3).

4 Conclusions

This manuscript reports the sample preparation route dependent relative changes in crystal phases and the degree of crystallinity of the PVA film, the PVA/PVP blend film, and their matrices based nanocomposites with varying concentration of the MMT nanofiller up to 10 wt%. The melt compounded films of both the pristine PVA and that of the PVA/PVP blend have high crystallinity and multiple crystal phases as compared to their single crystal phase solution cast prepared films. The presence of PVP in the melt compounded PVA/PVP blend film promotes the strength of $10\bar{1}$ phase concentration and simultaneously suppresses the 101 phase of the semicrystalline PVA in the blend film. The $10\bar{1}$ and 101 phases concentration exhibited their mutual alterations with the variation of MMT concentration in the PVA/*x* wt% MMT nanocomposites. The PVA crystals reflection planes in the PVA/PVP/*x* wt% MMT nanocomposites obey the characteristics of the melt compounded PVA film with a small variation in their crystallinity when MMT concentration was increased up to 10 wt%. The results revealed that the crystallite sizes of various crystals structures in the melt compounded PVA and PVA/PVP blend matrices based these nanocomposites vary anomalously in a wide range with the change of MMT concentration. The detailed structural parameters of the melt compounded PVA/*x* wt% MMT and PVA/PVP/*x* wt% MMT films reported in this paper could be interesting in view of structural modeling by the computer simulation for such type of inorganic-organic hybrid nanocomposite materials, and also in designing of flexible-type functional materials for their future technological applications.

Acknowledgement

The University Grants Commission, New Delhi, is gratefully acknowledged for the grant through SAP DRS-II Programme No. F.530/12/DRS-II/2016(SAP-I) sanctioned to the Department of Physics, JNV University, Jodhpur. One of the authors (PD) thanks the CSIR, New Delhi for award of postdoctoral research associate fellowship.

References

1 Pinnavaia T J & Beall G W, *Polymer-Clay Nanocomposites*, (Wiley), 2001.
2 Ray S S & Okamoto M, *Prog Polym Sci*, 28 (2003) 1539.
3 Ray S S & Okamoto M, *Prog Mater Sci*, 50 (2005) 962.
4 Mallakpour S & Rashidimoghadam S, *Hybrid Polym Compos Mater*, (2017) 227.
5 Buruga K, Song H, Shang J, Bolan N, Jagannathan, Kalathi T & Kim K H, *J. Hazardous Mater*, 379 (2019) 120584.
6 Rani P, Ahamed M B & Deshmukh K, *Polym Testing*, 91 (2020) 106744.
7 Dlamini D S, Li J & Mamba B B, *Appl Clay Sci*, 168 (2019) 21.
8 Jafarbeglou M, Abdouss M, Shoushtari A M & Jafarbeglou M, *RSC Adv*, 6 (2016) 50002.
9 Jlassi K, Chehimi M M & Thomas S, *Clay–Polymer Nanocomposites*, (Elsevier), 2017.
10 Guo F, Aryana S, Han Y & Jiao Y, *Appl Sci*, 8 (2018) 1696.
11 Sengwa R J, Choudhary S & Sankhla S, *Compos Sci Tech*, 70 (2010) 1621.
12 Choudhary S & Sengwa, R J, *J Appl Polym Sci*, 124 (2012) 4847.
13 Sengwa R J & Choudhary S, *Macromol Sym*, 362 (2016) 132.
14 Sengwa R J & Choudhary S, *J Appl Polym Sci*, 131 (2014) 40617.
15 Choudhary S & Sengwa R J, *J Appl Polym Sci*, 131 (2014) 39898.
16 Yu Y H, Lin C Y, Yeh J M & Lin W H, *Polymer*, 44 (2003) 3553.
17 Sengwa R J & Choudhary S, *Express Polym Lett*, 4 (2010) 559.
18 Sengwa R J, Choudhary S & Sankhla S, *Express Polym Lett*, 2 (2008) 800.
19 Sengwa R J, Choudhary S & Sankhla S, *Polym Int*, 58 (2009) 781.
20 Ali H E & Khairy Y, *Phys B*, 572 (2019) 256.
21 Soliman, T S, Vshivkov, S A & Elkalashy S I, *Polym Compos*, 41 (2020) 3340.
22 Choudhary S & Sengwa R J, *J Appl Polym Sci*, 134 (2017) 44568.
23 Dhatarwal P, Choudhary S & Sengwa R J, *Mater Lett*, 273 (2020) 127913.

24 Choudhary S, Dhatarwal P & Sengwa R J, *Indian J Chem Tech*, 27 (2020) 201.
25 Dhatarwal P & Sengwa R J, *J Macromol Sci B*, 59 (2020) 853.
26 Ambrosio R, Carrillo A, Mota M L, de la Torre K, Torrealba R, Moreno M, Vazquez H, Flores J & Vivaldo I, *Polymers*, 10 (2018) 1370
27 Assender H A & Windle H A, *Polymer*, 39 (1998) 4295.
28 Assender H A & Windle H A, *Polymer*, 39 (1998) 4303.
29 Strawhecker K E & Manias E, *Chem Mater*, 12 (2000) 2943.
30 Strawhecker K E & Manias E, *Macromolecules*, 34 **(**2001) 8475.
31 Sengwa, R.J. & Choudhary S. *Adv Mater Proc*, 2 (2017) 280.
32 Divyasree M C, Shiju E, Francis J, Anusha P T, Rao S V & Chandrasekharan K, *Mater Chem Phys*, 197 (2017) 208.
33 Wu Z, Wang T, Sun C, Liu P, Xia B, Zhang J, Liu Y & Gao D, *AIP Adv*, 7 (2017) 125213.
34 Sapalidis A A, Katsaros F K, Steriotis T A & Kanellopoulos N K, *J Appl Polym Sci*, 123 (2012) 1812.
35 Gaaz T S, Sulong A B, Akhtar M N, Kadhum A A H, Mohamad A B & Al-Amiery A A, *Molecules*, 20 (2015) 22833.
36 Mousa M & Dong Y, *Polymers*, 12 (2020) 264.
37 Chang J H, *Nanomaterials*, 9 (2019) 323.
38 Rad A S & Ebrahimi D, *Mechanics Compos Mater*, 53 (2017) 373.
39 Kim J M, Lee M H, Ko J A, Kang D H, Bae H & Park H J, *J Food Sci*, 83 (2018) 349.
40 Santos A J, Pina L T S, Galvão J G, Trindade G G G, Nunes R S, Santos J S, Santos C P, Gonsalves J K M C, Lira A A M, Cavalcanti S C H, Santos R L C, Sarmento V H V & Nunes R S, *Appl Clay Sci*, 185 (2020) 105394.
41 Sengwa R J & Sankhla S, *Polymer*, 48 (2007) 2737.
42 Hill D J T, Whittaker A K & Zainuddin, *Radiat Phys Chem*, 80 (2011) 213.
43 Sengwa R J, Sankhla S & Choudhary S, *Indian J Pure Appl Phys*, 48 (2010)196.
44 Freitas D F S, Mattos G C & Mendes L C, *J Therm Anal Calor*, 2020. DOI: 10.1007/s10973-020-09599-7
45 Choudhary S & Sengwa R J, *Curr Appl Phys*, 18 (2018) 1041.
46 Choudhary S, *J Mater Sci Mater Electron*, 29 (2018) 10517.
47 Choudhary S, *Polym Compos*, 39 (2018) E1788.